中國機械工程學刊第四十五卷第六期第 543~552 頁(民國一百一十三年)
Journal of the Chinese Society of Mechanical Engineers, Vol.45, No.6, pp543~552 (2024)

Fault Detection for Train Drive Shafts Based on Principal Component Analysis of Vibration Signals

Ping-Chun Tsai* and Ying-Chen Chuang**

Keywords：principal component analysis, MRT train, drive shaft, fault detection.

ABSTRACT

To develop a fault detecting model for monitoring the health of a drive shaft during operation of trains on Taipei's Wenhu train line, this study developed a train drive shaft fault detection method by using principal component analysis (PCA). First, numerous features were extracted from drive shaft vibration signals collected during train operation. Redundant features were removed through feature ranking, and PCA was used to reduce the features' dimensionality. The model was ultimately established using PCA and Hotelling's T^2 statistics. The proposed method is constructed using only vibration data from a healthy drive shaft. The feasibility of the proposed methodology was validated experimentally. The detection rate and false positive rate were 100% and 4.7%, respectively. The main contributions of this study are as follows: Interpretable drive shaft wear signals were identified. The diagnosis model is constructed entirely from measurements of healthy drive shafts. The model enables real-time drive shaft monitoring.

INTRODUCTION

The key components of a drive shaft in a mass rapid transit (MRT) railway vehicle are a rotary shaft, a ball socket base, a ball, and a shaft base. The ball is mounted on the shaft base and connected to the ball socket base, which transfers the engine torque from the rotary shaft to the differential. Over time, wear of the ball or ball socket base occurs. Internal statistics of the Taipei MRT Corporation (Metro Taipei) indicate that for the Taipei MRT system on Taipei's Wenhu train line, wear of the ball socket base is a main cause of MRT train failure. If the wear is excessive, the drive shaft may detach from the ball socket joint, resulting in the drive shaft idling and the train halting without warning. Such an event would be inconvenient and unsafe for passengers. Therefore, component monitoring and fault detection are critical to ensuring that railway vehicles are safe and reliable (Shah et al., 2021). Studies (Muszynska, 1995; Gangsar et al., 2021; Espinoza-Sepulveda and Sinha, 2021) have experimentally demonstrated that the vibration level is correlated with the health of the rotating shaft; abnormal states are associated with specific patterns that can be extracted from vibration signals (Tiboni et al., 2022).

Vibration measurement analysis has been used for railway vehicle transmission system diagnosis for many years; relevant recent studies have focused on various transmission system components, such as the gearbox or bearings (Yi et al., 2015; Huang et al., 2020; Bai et al., 2021; Xu et al., 2021; Luo et al., 2020). Few studies have discussed the vibration-based diagnosis of faults caused by ball nesting and ball wear of the drive shaft. Because the two ends of a drive shaft are connected to the traction motor and differential, respectively, drive shaft failure causes substantial vibration in the differential. Thus, information on the drive shaft and possible faults can be indirectly obtained by analyzing differential vibration (Yi et al., 2015).

However, the characteristics of vibration in a train transmission system are dynamic due to wheel-rail coupling excitation effects, which can result in force excitation (Zhai, 2015; Xu et al., 2018). Moreover, abnormal track sections, such as track gradient change points and track transitions, also result in vibration (Hamadache et al., 2019). Hence, due to the complexity of the transmission system's structure and the operating environment, measured transmission system vibration signals are often coupled (Qiao et al., 2021).

Features extracted from a measured signal must subsequently be selected on the basis of their

Paper Received November, 2023. Revised January, 2024. Accepted February, 2024. Author for Correspondence: Ping-Chun Tsai.

* *Department of Mechanical Design Engineering, National Formosa University, No. 64, Wunhua Rd., Huwei Township, Yunlin County 632, Taiwan (R.O.C.).*

** *Taoyuan Metro Corporation, No. 251, Sec. 4, Linghang N. Rd., Dayuan Dist., Taoyuan City 337, Taiwan (R.O.C.).*

importance if an accurate and generalizable model is to be obtained (Cheng et al., 2020). In fact, determining the number of features to be selected is another key step in feature selection. The dimensionality of the feature space that fully represents drive shaft failure is unknown; however, selecting an excessive number of features results in overfitting of the model (Verleysen and François, 2005). Besides, one challenge is faced when using such data driven methods: the physical meaning of mined features is often unclear (they are not interpretable), resulting in difficulty generalizing models or evaluating their robustness. Obtaining interpretable features is crucial for developing a general diagnosis model (Cheng et al., 2020).

Moreover, the samples used to train models are usually small because training datasets containing information on abnormal drive shaft operation are difficult to collect during a train's operation. Establishing accurate diagnostic models under such conditions and with limited data is challenging (Wang et al., 2021).

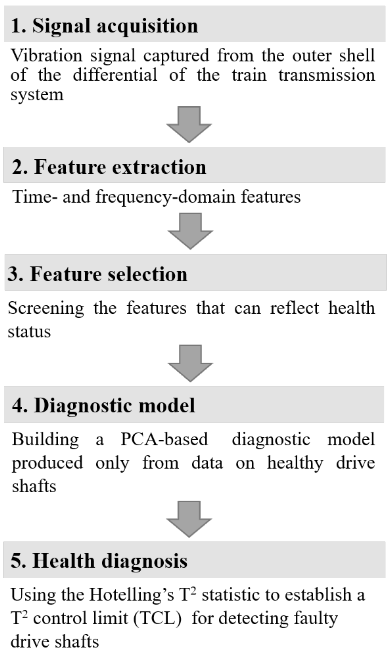

Fig. 1. Data analysis and establishing the diagnostic model.

To overcome this challenge, experiments were first conducted on the drive shafts of actual trains used on the MRT Wenhu Line to collect vibration data from healthy and faulty drive shafts. Subsequently, numerous time- and frequency-domain features were extracted. The diagnostic features were then found based on their importance to ensure the capability for detecting faulty drive shaft. In practical application, the method proposed in this study utilized these diagnostic features only from healthy drive shafts of in-service operating trains to establish an PCA-based unsupervised model. This model then employed corresponding Hotelling's T^2 statistics (Ahmed et al., 2012) to estimate the threshold for distinguishing between healthy and faulty drive shafts (Fig. 1). The remainder of this paper is structured as follows. Section 2 describes the experiments in which the vibration within an in-service train was measured. Vibration were measured using accelerometers mounted on the differential of the train's transmission system during train operation. Section 3 details the feature extraction, feature ranking, and PCA-based fault diagnosis. The verification of the proposed method by conducting an in-service train monitoring experiment is discussed in Section 4. Finally, Section 5 summarizes the results and contributions of this study.

EXPERIMENT DESCRIPTION

Problem Description

Numerous researchers have investigated the diagnosis of faults in train transmission systems; however, testing has been limited due to passenger safety considerations. Therefore, experiments are typically conducted using test rigs or numerical simulations instead of real trains (Huang et al., 2020; Bai et al., 2021; Xu et al., 2021; Luo et al., 2020). However, test rigs usually do not accurately replicate the complex operating environments of an actual vehicle; therefore, such methods may have low accuracy in practical applications.

In this study, experiments were conducted on the drive shaft of actual trains used on the MRT Wenhu Line with the cooperation of Metro Taipei; the study's goal was to develop an effective model for diagnosing faults in a train's drive shaft and that can be applied in practice. MRT trains on the Wenhu Line have a drive shaft (Model No. apt-312676-001) comprising a rotary shaft, ball socket base, ball, and shaft base (Fig. 2). The ball is mounted on the shaft base and connected to the ball socket base, which transfers engine torque from the rotary shaft to the differential. Abnormal vibration due to slight wear of the ball or ball socket base is difficult for passengers and train attendants to detect; initial drive shaft abnormality is thus typically ignored. However, increasing wear eventually results in the drive shaft detaching from the ball joint, resulting in the train coming to a stop without warning; this is dangerous for passengers.

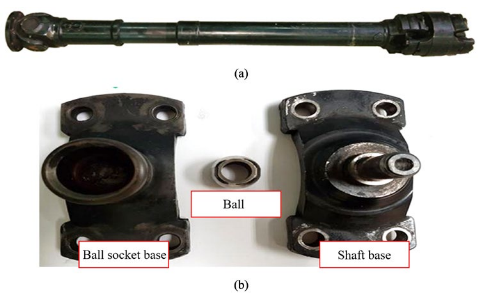

Fig. 2. Vehicle drive shaft: (a) rotary shaft and (b) ball socket base, ball, and shaft base.

Abnormal vibration due to ball socket base wear is transmitted from the drive shaft to the differential. Therefore, the vibration of the transmission system and the health of the drive shaft are closely related (Muszynska, 1995; Gangsar et al., 2021; Espinoza-Sepulveda and Sinha, 2021; Yi et al., 2015). To understand the relationship between the health of the drive shaft and its vibration, vibration tests were conducted on operating trains by installing an accelerometer on the body of the differential; the relevant features of the drive shaft's vibration were then analyzed.

Real Vehicle Data Collection

Vibration data were measured using a uniaxial piezoelectric accelerometer (NOVA NV-1202) mounted on the outer shell of the differential (Fig. 3) of a vehicle. The accelerometer specifications are presented in Table 1. The signal acquisition module was PROWAVE UAQ21 (Table 2). Signal analysis and processing were performed using MATLAB. The vibration signal measurements had a sampling rate of 7324 Hz.

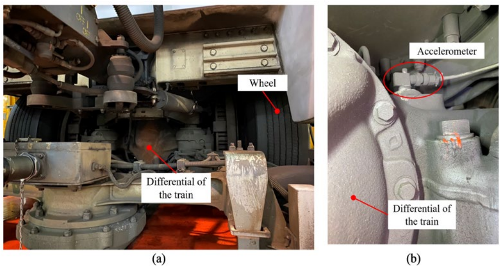

Fig. 3. Differential vibration measurement setup: (a) vehicle chassis and differential and (b) accelerometer installation.

Table 1. Accelerometer specifications (NOVA NV-1202).

Parameter	Value
Sensitivity	100 mV/g
Frequency response (±3dB)	0.5 ~ 10000 Hz
Measuring range	±50 g
Noise	< 50μV

Table 2. Data acquisition module specifications (PROWAVE UAQ21).

Parameter	Value
Input Range	100 mV/g
Maximal Sampling rate	28 kHz
Resolution	24 bits
Built-in filter	Anti-aliasing filter
Input configuration	IEPE

Wenhu line trains comprise two linked trainsets facing opposite directions. Tests were performed simultaneously on two trainsets linked to form a complete train: a reference trainset with a healthy drive shaft (reference trainset), and a faulty trainset with a worn-out ball in its drive shaft's ball socket base (faulty trainset). The wear and peeling on the surface of the ball were clearly visible (Fig. 4). Vibration signals from both drive shafts were collected simultaneously while the train was in motion. This setup ensured that the routes, motion conditions, and environmental conditions (e.g., weather) for the two trainsets were nearly identical; ensuring the reliability of the measurement data and the generalizability of the developed model.

Fig. 4. Comparison of a normal ball with a worn ball.

Due to operational considerations by Metro Taipei, only vibration signals from the track section between the Songshan Airport and Dazhi stations were analyzed. However, the train accelerates, decelerates, and travels at constant speed at various points in this section; some sections are straight and others are curved. Changes in train speed due to acceleration or turns may produce vibration signals with irregular characteristics (Hu et al., 2021). Therefore, feature extraction and subsequent analysis were only performed for vibration signals generated during constant-speed (70.7 km/h) straight motion. This means that the diagnostic model subsequently developed can only be applied to make predictions for this particular section. If the driving track sections or conditions change, the detection model needs to be re-established.

Experimental Results

The drive shaft health diagnosis experiments were performed on various dates between October 21 and December 1, 2021 (Table 3). A total of 430 data files were obtained; of these, 234 and 196 were from the reference and faulty trainsets, respectively. Each data file was a 1.118-second vibration signal recorded at 70.7 km/h with a sampling rate of 7324 Hz, meaning that there were 8192 data points. The files were divided into four subdatasets: A, B, C, and D. Datasets A and C were captured from the healthy drive shaft, whereas datasets B and D were captured from the faulty one. Time- and frequency-domain features were extracted from datasets A and B and then ranked. Dataset A was also used for PCA. Datasets C and D were used for model testing. Data were collected on 41 days to ensure that the datasets included data affected by various planned environmental factors, such as different weather conditions, weekdays, holidays, as well as morning peak hours and evening off-peak hours. This approach was taken to ensure the robustness of the feature selection and the detection model.

Table 3. Details of the four subdatasets.

Sub-dataset	Number of data	Experimental date	Status of drive shaft
A	148	10/21, 10/26, 11/1~11/8	Healthy
B	114	11/3~11/8	Failure
C	86	11/9~11/11, 12/1	Healthy
D	82	11/9~11/11, 12/1	Failure

FAULT DIAGNOSIS MODELLING BASED ON PCA

Characteristic Vibration Frequency Analysis

Figure 5 presents the transmission system structure of a Wenhu Line train. The torque generated from the engine is transmitted to the wheels through the drive shaft, differential, axle shaft, and hub reductor in turn. When the drive shaft fails, abnormal vibrations can be measured by an accelerometer installed on the differential. The theoretical frequency of the drive shaft vibration characteristics can be obtained on the basis of parameters such as the speed reduction ratio of the transmission system and train speed (70.7 km/h), as shown in Table 4. For an abnormal drive shaft, the vibration signal related to its characteristic frequency is expected to differ from that of a healthy drive shaft.

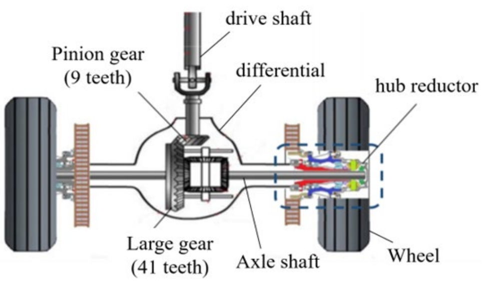

Fig. 5. Train transmission system.

Table 4. Vibration characteristic frequencies of the transmission system.

Transmission components	Frequency (Hz)
Drive shaft (f_d)	58
mesh frequency of the pinion gear and large gear in the differential (f_m)	522
Rotating frequency of axle shaft (f_a)	12.8
Rotating frequency of wheel (f_w)	6.4

To understand the relationship between the vibration characteristics of the drive shaft and its health, a simple comparison of the vibration spectra of the healthy and faulty drive shafts, obtained through the fast Fourier transform (FFT), is presented in Fig. 6; the two vibration spectra clearly differ. The dominant vibrations were at 522 Hz, which was the mesh frequency of the driving gear and driven gear (f_m), and also its harmonic $2 \times f_m$ at 1045 Hz. Because the driving gear is directly connected to the drive shaft, abnormal vibrations in a faulty drive shaft usually affect the amplitude of f_m. Moreover, the frequency amplitudes in the faulty drive shaft spectrum were larger than those in the healthy drive shaft spectrum over the frequencies of 3038–3255 Hz. In addition, it can be observed that the amplitude of the fundamental drive shaft rotation frequency (f_d) of the faulty drive shaft is 1.8 times that of a healthy drive shaft. This indicates that relying on the characteristics of vibration signals to identify the health status of drive shafts is feasible.

However, relevant signal characteristics in the spectrum may be subject to noise interference; therefore, determining the fault condition solely on the basis of the spectrum's peaks is challenging when using an intuitive analysis. To more accurately determine fault status, vibration signal features can be obtained and ranked using various algorithmic methods.

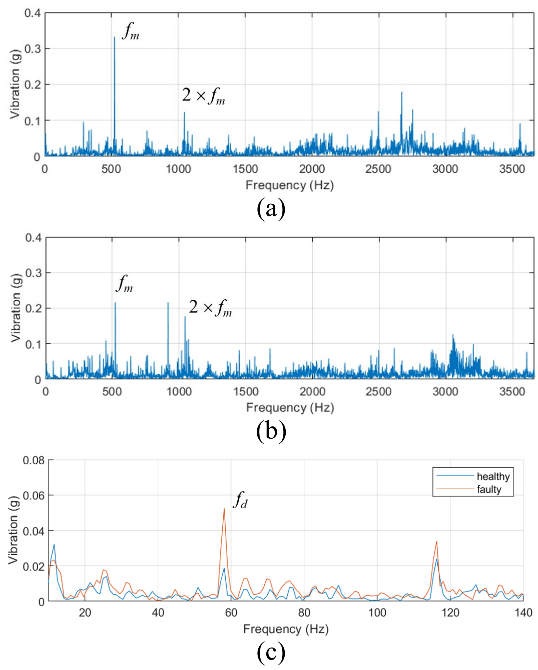

Fig. 6. Comparison of FFT spectra for a (a) healthy, (b) faulty drive shaft and (c) the amplitudes of the fundamental drive shaft rotation frequency.

Signal Feature Extraction Methods

In a rotary machine system, the vibration spectra due to wear generally contain harmonic frequencies (e.g., 2 × RPM, 3 × RPM) and fractional frequencies (e.g., 1/2 × RPM, 1/3 × RPM, 1/4 × RPM); the rotational frequency (in RPM) is the fundamental frequency of the rotary machine system (Moble, 1999; Chu and Lu, 2005). For a railway vehicle transmission system with a worn ball or ball socket base, the rotational frequency of the drive shaft (f_d = 58 Hz) can be regarded as the fundamental frequency. As wear increases, the ball joint loosens, often resulting in subharmonic frequencies such as 0.5 × f_d, 1.5 × f_d, or 2.5 × f_d (Moble, 1999; Chu and Lu, 2005). In other words, abnormal friction, relative motion, or collisions between the worn ball and ball socket base may affect the amplitudes of the harmonic or subharmonic frequencies of f_d. In addition, due to the excitation of vibrations caused by worn parts, higher amplitudes and more sidebands surrounding the harmonic frequencies of f_d were expected to be present in the worn-shaft signal. Sidebands may be better wear indicators than the harmonic frequencies of f_d. However, predicting which harmonic frequencies, subharmonic frequencies, or sidebands will be present in the vibration spectra as the ball or ball socket base wears out is challenging.

Table 5 presents the 104 features that were extracted. The time-domain features include the RMS amplitude, kurtosis (KUR), skewness (SKE), standard deviation (STD), and crest factor (CF) of the signals. The frequency-domain features were the amplitudes (M) corresponding to the rotation frequency of the drive shaft (f_d = 58 Hz), its harmonic frequencies (2 × f_d, …, 7 × f_d) and subharmonic frequencies (0.5 × f_d, 1.5 × f_d, …, 7.5 × f_d) as well as the sum of the amplitudes of the specific frequency region (band energy, BE) and the BE proportion (BEP). $\mathrm{M}_{n\mathrm{X}}$ represents the amplitude in the vibration spectrum of the transmission system at $n \times f_d$, where n is an integer. Changes in the amplitude and number of sidebands were quantified using the BE and BEP. The BE was calculated by dividing the spectrum from 55 to 455 Hz into 40 nonoverlapping 10-Hz frequency bands and summing the amplitudes; the BEP was the ratio between this sum and that of the entire spectrum. For example, $\mathrm{BE}_{[55,65]}$ represents the sum of amplitudes from 55 to 65 Hz; $\mathrm{BE}_{[55,455]}$ represents the sum of amplitudes from 55 to 455 Hz; and $\mathrm{BEP}_{[55,65]}$ represents the ratio of $\mathrm{BE}_{[55,65]}$ to $\mathrm{BE}_{[55,455]}$. The BE indicates the absolute amplitudes of a frequency band; the BEP represents the amplitude of that frequency band in relation to that of the entire spectrum. These frequency-domain features were selected to avoid the vibration characteristic frequencies (and their harmonics, Table 4) of other components in the transmission system, such as the differential, pinion gear, large gear, axle shaft, and wheel; this ensured that the extracted frequency-domain features (Table 5) were only related to the vibration characteristics of the drive shaft.

Table 5. Extracted features.

Features	Expression	Description
RMS	$\sqrt{\frac{1}{N}\sum_{i=1}^{N} x_i^2}$	Root mean square
STD	$\frac{1}{N}\sum_{i=1}^{N}(x_i-\overline{x})^2$	Standard deviation
SKE	$\frac{\sum_{i=1}^{N}(x_i-\overline{x})^3}{N(\mathrm{STD})^3}$	Skewness
KUR	$\frac{\sum_{i=1}^{N}(x_i-\overline{x})^4}{N(\mathrm{STD})^4}$	Kurtosis
CF	$\frac{\max(x_i)}{\mathrm{RMS}}$	Crest factor
$\mathrm{M}_{n\mathrm{X}}$	$s(n\times f_d), n=1,1.5,2,\ldots,7.5$	Amplitudes corresponding to the harmonic and sub-harmonic frequency of f_d
$\mathrm{BE}_{[f1,f2]}$	$\sum_{k=f_1}^{f_2} s(k), f_1=55,65,\ldots,445; f_2=f_1+10$	Sum of the amplitudes of the spectrum region from f_1 to f_2 Hz
$\mathrm{BEP}_{[f1,f2]}$	$\frac{\mathrm{BE}_{[f_1,f_2]}}{\mathrm{BE}_{[55,455]}}, f_1=55,65,\ldots,445; f_2=f_1+10$	The ratio of $\mathrm{BE}_{[f1,f2]}$ to $\mathrm{BE}_{[55,455]}$

Note: $x_i = (x_1, x_2, \ldots, x_N)$ is the sequence of time-domain signal; $s(k)$ is the amplitude corresponding to the frequency of k Hz in fast Fourier transform (FFT) spectrum of x_i.

Feature Selection and Modelling for Fault Diagnosis

The Fisher criteria (Gan and Zhang, 2021) were selected for feature ranking in this study because this method evaluates the importance of features on the basis of only their ability to distinguish whether a drive shaft is healthy or faulty. Thus, environmental factors (train load, direction of travel, weather conditions, etc.) were unlikely to influence the ranking. However, the key features obtained using the Fisher criteria may be colinear and therefore the set of these features may have redundancy (Shekar et al., 2017). PCA was used to reduce the dimensions of the feature dataset by eliminating colinearity between features.

Using PCA for condition monitoring involves two stages: in Stage 1, construct a PCA model on the basis of the training feature dataset; in Stage 2, apply the PCA model to a feature dataset produced from new observations. In Stage 1, for a z-score (Patro and Sahu, 2015) standardized feature dataset $\mathbf{X} \in \Re^{m \times n}$ of m samples and n variables (i.e., features obtained from healthy vibration signals), which could be decomposed as follows:

$$\mathbf{X} = \mathbf{t}\mathbf{P}^{\mathrm{T}}, \tag{1}$$

where $\mathbf{P} = [\mathbf{p}_1 \ \cdots \ \mathbf{p}_i \ \cdots \ \mathbf{p}_n]$ is defined as the principal component (PC) loading matrix and $\mathbf{t} = [\mathbf{t}_1 \ \cdots \ \mathbf{t}_i \ \cdots \ \mathbf{t}_n]$ is defined as the score matrix of the PCs. The PC loading vector $\mathbf{p}_i$ is an eigenvector of the correlation matrix of $\mathbf{X}$, and the corresponding eigenvalue is denoted as λ_i. This eigenvalue was used to measure the importance of the corresponding PC loading vector. Features with low importance or that were redundant had small eigenvalues and could be ignored. The contribution f_j of each PC loading vector could be quantified by computing the ratio of its eigenvalue to the sum of all eigenvalues (Ahmed et al., 2012). In Stage 2, the standardized feature dataset $\mathbf{X}_{\text{new}}$ of new observations was then projected onto the PC loading vectors of the original PCA model to obtain a corresponding score vector $\mathbf{t}'_i$ as follows:

$$\mathbf{t}'_i = \mathbf{X}_{\text{new}}\mathbf{p}_i,\ i = 1, 2, \ldots n. \tag{2}$$

Hotelling's T^2 statistic is a PCA-based fault detection index (Ahmed et al., 2012), it is computed by discarding the PC loading vectors with lower contributions and keeping only the top k vectors:

$$\mathbf{T}^2 = \sum_{j=1}^{k} \frac{(\mathbf{t}'_j)^2}{\lambda_j}, \tag{3}$$

where λ_j are the k largest eigenvalues of the correlation matrix of $\mathbf{X}$ in Eq. (1), and $\mathbf{t}'_j$ is the jth PC score vector obtained from Eq. (2). The training dataset used to construct the PCA model was from a healthy drive shaft of the train; therefore, the Hotelling's T^2 statistic for a healthy drive shaft could be obtained by transforming the training data using Eqs. (2) and (3); these statistics are denoted the T^2 baseline model, which representing the pattern of a healthy drive shaft and can quantify the boundary between healthy and abnormal drive shafts. By comparing novel samples with the trained baseline model, these samples could be classified as normal or faulty.

RESULTS AND DISCUSSION

Results of Feature Ranking and Screening

The feature datasets for the four experimental subdatasets A, B, C, and D were obtained using the feature extraction method described in Section 3.2; Feature importance ranking was performed for feature datasets A and B as shown in Fig. 7. The three most highly ranked features had substantially higher Fisher scores and were therefore retained (Table 6); the remaining features were discarded. The three selected features were related to the drive shaft rotation frequency. The highest-ranked feature, M_{1X}, was the amplitude of the fundamental drive shaft rotation frequency ($1 \times f_d$). Thus, the amplitude of $1 \times f_d$ changed considerably as the ball or ball socket base wore; this was attributed to increased ball–socket clearance. The second- and third-ranked features, $BEP_{[55,65]}$ and $BE_{[55,65]}$, were related to the frequency band including $1 \times f_d$. Thus, ball and ball socket base wear not only caused a major increase in amplitude at $1 \times f_d$ but also around this frequency. These features could be interpretable in terms of the drive shaft mechanism. The screened three features, M_{1X}, $BEP_{[55,65]}$, and $BE_{[55,65]}$, were extracted from subdatasets A, B, C, and D to obtain three corresponding feature datasets A^*, B^*, C^*, and D^*.

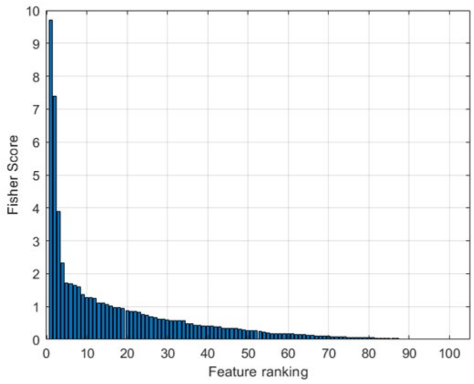

Fig. 7. Fisher feature ranking results.

Table 6. Features selected on the basis of their Fisher feature ranking.

Rank	Feature	Description
1	M_{1X}	Amplitude of the spectrum at $1 \times f_d$ (f_d = 58 Hz)
2	$BEP_{[55,65]}$	The ratio of $BE_{[55,65]}$ to $BE_{[55,455]}$
3	$BE_{[55,65]}$	Sum of the amplitudes of the spectrum region from 55 to 65 Hz

PCA Model Development

PCA was applied to feature dataset A* to construct a model, the performance of which was verified on feature datasets C* and D*. Figure 8 presents the overall training and testing process. Elements of A* were randomly grouped into two datasets (A1 and A2) at a ratio of 1:1, and these datasets were used for training and testing the trained PCA model, respectively. The corresponding T^2 baseline (i.e., the Hotelling's T^2 statistic of the healthy drive shaft) could be obtained for drive shaft diagnosis.

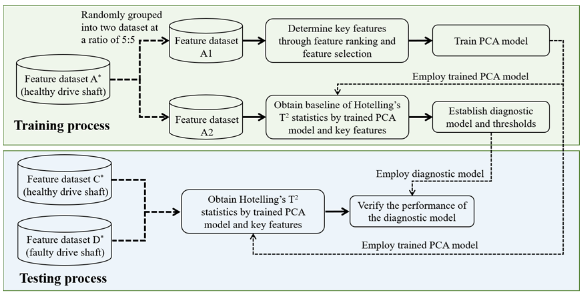

Fig. 8. Training and testing with the feature datasets A*, C*, and D*.

Figure 9 presents the contributions of the PC loading vectors. The two largest PCs accounted for 95% of the cumulative contribution; thus, the subspace comprising only PC1 and PC2 contained sufficient information about the original features to diagnose drive shaft faults. Due to space limitations, the method of selecting the number of PCs is not discussed here but can be found in Jolliffe (1982).

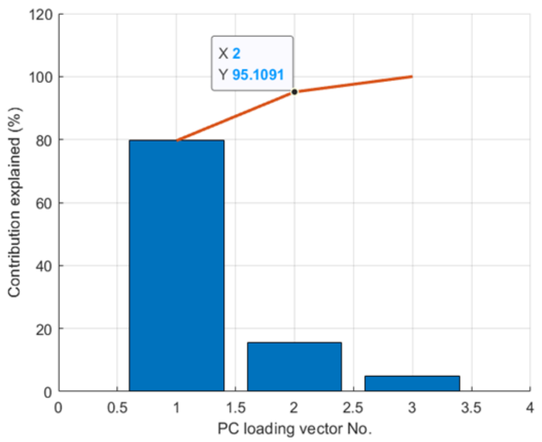

Fig. 9. PC loading vector selection.

Drive Shaft Diagnostic Model

The feature dataset A2 was used along with the developed PCA model and corresponding Hotelling's T^2 statistic to establish a threshold for differentiating healthy from faulty engines. If the T^2 statistic of novel observations exceeds this threshold, a drive shaft is identified as abnormal. This threshold is denoted the T^2 control limit (TCL) and was set as three standard deviations greater than the mean T^2 baseline value:

$$\mathrm{TCL} = \mu + 3\sigma, \tag{4}$$

where σ and μ are the standard deviation and the mean value of the data of T^2 baseline, respectively. Previous studies have demonstrated that statistical thresholds of Hotelling's T^2 statistic can be calculated using the F-distribution as follows (Ahmed et al., 2012):

$$T_\alpha = \frac{k(m-1)}{m-k} F_\alpha(k, m-k), \tag{5}$$

where T_α is the threshold with confidence level α of 95% or 99%, k is the number of PCs retained in the PCA model; m is the number of samples used in PCA; and $F_\alpha(k, m-k)$ is the upper $(100 \times \alpha)$% limit of the F-distribution with k and $(m-k)$ degrees of freedom. The statistical threshold T_α with the selected confidence level 95% or 99% (i.e., $T_{\alpha,95}$ and $T_{\alpha,99}$) could be estimated using Eq. (5).

Diagnosis Results and Discussion

The feature datasets C* (healthy) and D* (faulty)—containing 86 and 82 data points, respectively—were used to verify the performance of the model. The Hotelling's T^2 statistics of C* and D* was obtained for the thresholds of TCL, $T_{\alpha,95}$, and $T_{\alpha,99}$. Figure 10 presents the confusion matrices (Fawcett, 2006) for the three diagnostic thresholds. The labels 0 and 1 indicate healthy and faulty drives, respectively. Figure 10 reveals that $T_{\alpha,95}$ had the lowest accuracy, whereas TCL had the highest accuracy. The faulty drive shafts were all correctly classified. The classification accuracies for test datasets C and D when using TCL, $T_{\alpha,95}$, and $T_{\alpha,99}$ as the diagnostic threshold are 97.62%, 92.26%, and 96.43%, respectively; the precisions are 95.3%, 86.3%, and 93.2% respectively; and the recall rates are all 100%. The proposed threshold, TCL, had the highest classification accuracy. In fact, diagnostic thresholds based on statistical standard deviations or F-distributions often erroneously categorize outliers; this is a common challenge encountered when constructing diagnostic models on the basis of only healthy datasets.

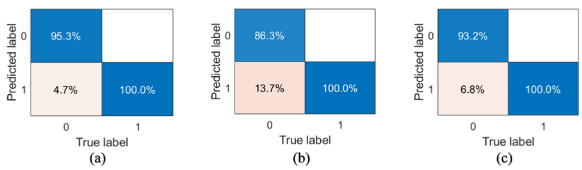

Fig. 10. Confusion matrix of the diagnostic model when using the three diagnostic thresholds: (a)TCL, (b) $T_{\alpha,95}$, and (c) $T_{\alpha,99}$. *Note: Label 0 means the status of the drive shaft is healthy, label 1 means faulty.

In addition, the classification accuracy for differentiating healthy and faulty drive shafts through the proposed methodology (i.e., the PCA-based unsupervised learning model and TCL) and Support vector machine (SVM) (Borhana et al., 2020) was also compared. SVM with Radial basis function (RBF) kernel was applied to feature dataset A^* and B^* to construct a classification model, the performance of which was verified on feature datasets C^* and D^*. Although supervised machine learning methods such as SVM can recognize the health of drive shafts with 98.81% accuracy, training these models requires obtaining data on both healthy and faulty drive shafts. By contrast, although the accuracy of the proposed method was 1.19% lower than that of the test SVM, the diagnostic model and judgment threshold, the TCL, can be established on the basis of the vibration signals captured from only a healthy drive shaft; data from a faulty drive shaft are unnecessary.

CONCLUSIONS

For train drive shafts, the objective is to develop a model for monitoring the health of a drive shaft during operation of trains on Taipei's Wenhu train line. For this, a train drive shaft fault detection method by using PCA and TCL was proposed in this study. The following conclusions can be drawn:

1. Experiments were conducted on the trains used on the MRT Wenhu Line that were in actual service; a diagnostic model was developed to detect faults in the drive shafts, and it is capable of being applied in practice.
2. The experimental results of the feature analysis and importance ranking indicate that the amplitude of the vibration spectrum at 58 Hz (i.e., the rotation frequency of the drive shaft), the sum of the amplitudes in the spectral region from 55 to 65 Hz ($BE_{[55,65]}$), and the ratio of $BE_{[55,65]}$ to $BE_{[55,455]}$ ($BEP_{[55,65]}$), were identified as key features detecting drive shaft faults. The three selected features were highly related to the drive shaft rotation frequency.
3. The classification accuracy when using the TCL, $T_{\alpha,95}$, and $T_{\alpha,99}$ as the diagnostic threshold were 97.62%, 92.26%, and 96.43%, respectively; the precisions are 95.3%, 86.3%, and 93.2% respectively; and the recall rates are all 100%. The statistical thresholds of Hotelling's T^2 statistic (i.e., $T_{\alpha,95}$ and $T_{\alpha,99}$) were estimated on the basis of the F-distribution, which is unaffected by actual measurement data. By contrast, the proposed threshold TCL was based on actual healthy drive shaft data and is thus more practically applicable. The detection rate and false alarm rate of using TCL were 100% and 4.7%, respectively.
4. The classification accuracy using the proposed method was 2.38% lower than SVM, however, a diagnostic model and judgement threshold TCL can be established on the basis of only vibration signals captured from a healthy drive shaft; data from a faulty drive shaft are unnecessary. In light of this, a methodology of monitoring drive shaft health for a newly installed healthy train drive shaft and based on the proposed approach is depicted in Fig. 11. A training data set is collected from a newly installed healthy drive shaft. A PCA model and a diagnostic model of drive shaft health are developed. Once regular operation begins, the PCA model and the Hotelling's T^2 statistic can be used to quantify the health status of the drive shaft through comparison with the diagnostic threshold TCL. This system can automatically establish a drive shaft fault detection model from an in-service operating train, and enables long-term, inexpensive monitoring of drive shaft health.

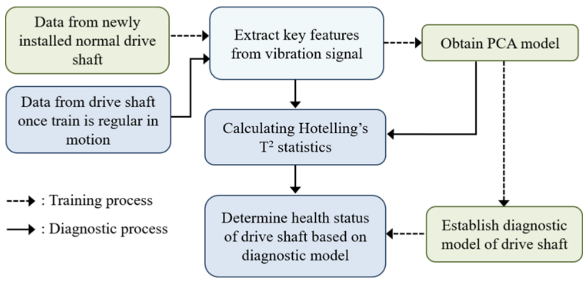

Fig. 11. Methodology for automatically diagnosing the health status of a drive shaft in a railway vehicle.

ACKNOWLEDGMENT

This study was supported by the Taipei Rapid Transit Corporation and the National Science and Technology Council, Taiwan, ROC (under Contract No. NSTC 110-2222-E-032-006-MY2).

REFERENCES

Ahmed, M., Baqqar, M., Gu, F. and Ball, A.D., "Fault Detection and Diagnosis Using Principal Component Analysis of Vibration Data From a Reciprocating Compressor," *Proceedings of 2012 UKACC International Conference on Control*, IEEE, pp. 461-466 (2012).

Bai, Y., Yang, J., Wang, J., Zhao, Y. and Li, Q., "Image Representation of Vibration Signals and Its Application in Intelligent Compound Fault Diagnosis in Railway Vehicle Wheelset-axlebox Assemblies," *Mechanical Systems and Signal Processing*, Vol. 152, p. 107421 (2021).

Borhana, A.A., Kamal, D.D.B.M., Latif, S.D., Ali, Y.H., Almahfoodh, A.N.A. and El-Shafie, A., "Fault Detection of Bearing Using Support Vector Machine-SVM," *2020 8th International Conference on Information Technology and Multimedia*, Selangor, Malaysia, pp. 309-315 (2020).

Cheng, W.N., Cheng, C.C., Lei, Y.H. and Tsai, P.C., "Feature Selection for Predicting Tool Wear of Machine Tools," *Int. J. Adv. Manufact. Technol.*, Vol. 111, No. 5, pp. 1483-1501 (2020).

Chu, F. and Lu, W., "Experimental Observation of Nonlinear Vibrations in a Rub-impact Rotor System," *J. Sound Vibrat.*, Vol. 283, No. 3-5, pp. 621-643 (2005).

Espinoza-Sepulveda, N., Sinha, J., "Mathematical Validation of Experimentally Optimised Parameters Used in a Vibration-based Machine-learning Model for Fault Diagnosis in Rotating Machines," *Machines*, Vol. 9, No. 8, p. 155 (2021).

Fawcett, T., "An Introduction to ROC Analysis," *Pattern Recogn. Lett.*, Vol. 27, No. 8, pp. 861-874 (2006).

Gangsar, P., Pandey, R.K. and Chouksey, M., "Unbalance Detection in Rotating Machinery Based on Support Vector Machine Using Time and Frequency Domain Vibration Features," *Noise Vibrat. Worldwide*, Vol. 52, No. 4–5, pp. 75-85 (2021).

Gan, M. and Zhang, L., "Iteratively Local Fisher Score for Feature Selection," *Appl. Intell.*, Vol. 51, No. 8, pp. 6167-6181 (2021).

Hamadache, M., Dutta, S., Olaby, O., Ambur, R., Stewart, E. and Dixon, R., "On the Fault Detection and Diagnosis of Railway Switch and Crossing Systems: An Overview," *Appl. Sci.*, Vol. 9, No. 23, p. 5129 (2019).

Huang, Y., Huang, C., Ding, J. and Liu, Z., "Fault Diagnosis on Railway Vehicle Bearing Based on Fast Extended Singular Value Decomposition Packet," *Measurement*, Vol. 152, p. 107277 (2020).

Hu, Z., Yang, J., Yao, D., Wang, J. and Bai, Y., "Subway Gearbox Fault Diagnosis Algorithm Based on Adaptive Spline Impact Suppression," *Entropy*, Vol. 23, No. 6, p. 660 (2021).

Jolliffe, I.T., "A Note on the Use of Principal Components in Regression," *J. R. Stat. Soc. Ser. C*, Vol. 31, No. 3, pp. 300-303 (1982).

Luo, H., Bo, L., Peng, C. and Hou, D., "Fault Diagnosis for High-speed Train Axle-box Bearing Using Simplified Shallow Information Fusion Convolutional Neural Network," *Sensors*, Vol. 20, No. 17, p. 4930 (2020).

Mobley, R.K., *Vibration Fundamentals*, Butterworth-Heinemann (1999).

Muszynska, A., "Vibrational diagnostics of rotating machinery malfunctions," *Int. J. Rotat. Mach.*, Vol. 1, pp. 237-266 (1995).

Patro, S.G.K. and Sahu, K.K., "Normalization: A Preprocessing Stage," arXiv preprint arXiv:1503.06462 (2015).

Qiao, N., Zhao, L., Liu, Y., Chen, Q., Hou, H. and Peng, T., "Research on Intelligent Diagnosis of Rail Vehicle Transmission System," *The 5th CAA International Conference on Vehicular Control and Intelligence*, pp. 1-5 (2021).

Shah, A.A., Bhatti, N.A., Dev, K. and Chowdhry, B.S., "MUHAFIZ: IoT-based Track Recording Vehicle for the Damage Analysis of the Railway Track," *IEEE Internet Things J.*, Vol. 8, No. 11, pp. 9397-9406 (2021).

Shekar, K., Bocklisch, T., Sánchez, P.I., Straehle, C.N. and Müller, E., "Including Multi-feature Interactions and Redundancy for Feature Ranking in Mixed Datasets," *Joint European Conference on Machine Learning and Knowledge Discovery in Databases*, LNAI (10534), pp. 239-255 (2017).

Tiboni, M., Remino, C., Bussola, R. and Amici, C., "A Review on Vibration-based Condition Monitoring of Rotating Machinery," *Appl. Sci.*, Vol. 12, No. 3, p. 972 (2022).

Verleysen, M. and François, D., "The Curse of Dimensionality in Data Mining and Time Series Prediction," *International Work-Conference on Artificial Neural Networks*, LNCS (3512), pp. 758-770 (2005).

Wang, J., Yang, J., Wang, Y., Bai, Y., Zhang, T. and Yao, D., "Ensemble Decision Approach With Dislocated Time-frequency Representation and Pre-trained CNN for Fault Diagnosis of Railway Vehicle Gearboxes Under Variable Conditions," *Int. J. Rail Transp.*, pp. 1-19 (2021).

Xu, G., Hou, D., Qi, H. and Bo, L., "High-speed Train Wheel Set Bearing Fault Diagnosis and Prognostics: A New Prognostic Model Based on Extendable Useful Life," *Mechan. Syst. Signal Process.*, Vol. 146, p. 107050 (2021).

Xu, L., Zhai, W. and Gao, J., "Global Sensitivity Analysis for Vehicle–track Interactions: Special Attention on Track Irregularities," *J. Comput. Nonlinear Dynam.*, Vol. 13, No. 3, p. 031007 (2018).

Yi, C., Lin, J., Ruan, T. and Li, Y., "Real Time Cardan Shaft State Estimation of High-speed Train Based on Ensemble Empirical Mode Decomposition," *Shock Vibrat.*, p. 912483 (2015).

Zhai, W.M., *Vehicle-track Coupling Dynamics*, Science Press, Beijing (2015).

基於振動訊號主成份分析之列車傳動軸故障檢測

蔡秉均
國立虎尾科技大學機械設計工程系

莊英震
桃園大眾捷運股份有限公司

摘 要

為了發展一種可在台北捷運文湖線列車行進過程中監測傳動軸健康狀況的故障檢測模型，本研究利用主成分分析（PCA）開發了一種列車傳動軸故障檢測方法。首先，從列車行進過程間所收集的傳動軸振動訊號中提取了多種具有用於建立診斷模型潛力的大量特徵，接著透過特徵重要性排序移除冗餘特徵後再使用 PCA 來降低其特徵空間的維度，並使用霍特林 T2 統計量建立診斷模型。所提出的方法僅使用來自健康傳動軸的振動數據構建，且診斷模型的可行性通過實驗得到了驗證，檢測率與假陽性率分別為 100%和 4.7%。本研究的主要貢獻為用於偵測傳動軸健康狀態之特徵具有可解釋性，且診斷模型完全由健康傳動軸的量測數據所構建，不需要額外收集故障傳動軸之數據。